Materials Transactions, Vol. 50, No. 8 (2009) pp. 1919 to 1923

Morphology and Crystallography of Sub-Blocks in Ultra-Low Carbon Lath Martensite Steel

S. Morito[1], Y. Adachi[2] and T. Ohba[1]

[1]*Department of Materials Science and Engineering, Shimane University, Matsue 690-8504, Japan*
[2]*Innovative Materials Engineering Laboratory, National Institute for Materials Science, Tsukuba 305-0047, Japan*

The morphology and crystallography of sub-blocks in lath martensite were studied in an interstitial free steel. In each block the sub-blocks are classified into dominant and minor sub-blocks in terms of the volume fraction. The orientation relationship between the dominant and minor sub-blocks is $[011]\alpha'/10.5$ degrees. Minor sub-blocks have a plate-like morphology and are connected to each other with the habit plane close to $\{111\}\gamma$, and their growth directions close to $\langle 10\bar{1}\rangle\gamma$. [doi:10.2320/matertrans.MRA2008409]

(Received November 4, 2008; Accepted May 7, 2009; Published June 24, 2009)

Keywords: *lath martensite, three-dimensional analysis, morphology, crystallography*

1. Introduction

Lath martensite (α') in steel is well known to show a hierarchical microstructure consisting of packets, blocks, sub-blocks, and laths. The prior austenite grain is divided into packets that consist of blocks. These blocks in a packet have the same habit plane. The packet is further divided into plate-like blocks, which consist of laths with a similar crystal orientation. Recently, it has been recognized that a block contains components called sub-blocks, each of which corresponds to a single variant characterized by the Kurdjumov–Sachs (K–S) orientation relationship with austenite (γ), as shown in Fig. 1.[1,2)]

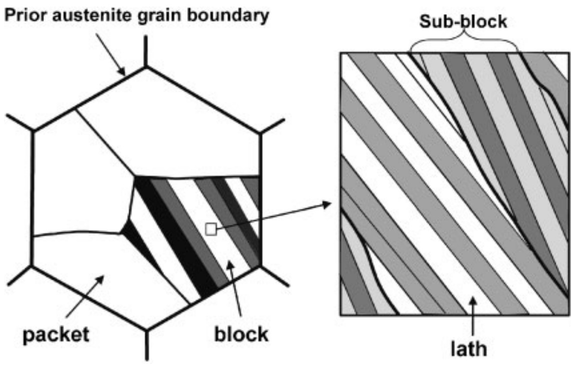

Fig. 1 Schematic illustration of lath martensite.[2)]

Complex morphology of lath martensite affects the toughness and strength of a high strength steel.[3,4)] It has been reported that the sub-block boundaries work as barriers to dislocation gliding, and eventually increase the strength of the lath martensite steel, although the sub-block boundaries are low angle boundaries.[5)] However, the morphology of the sub-block has not been fully characterized because of its fine size (about 7 µm) in interstitial free steel.[2)] Furthermore, the morphology of the sub-blocks varies even for those aligned along the same direction. Recently, three-dimensional (3D) tomography has been developed for metals, which enables characterization of the 3D morphology of complicated microstructures.[6,7)] Thus, 3D visualization is expected to provide new understanding of the characteristics of the sub-blocks.

This study aims to identify the morphology and crystallography of sub-blocks using two-dimensional (2D) and 3D analyses by scanning electron microscopy (SEM) equipped with an electron backscattering diffraction (EBSD) detector.

2. Experimental Procedure

The steel used in this study has the following chemical composition: Fe-0.0049 mass%C-3.14 mass%Mn-0.011 mass%Nb-0.021 mass%Ti-0.0025 mass%B. In order to obtain the lath martensite structure, specimens with a size of $10 \times 10 \times 5$ mm were austenitized at 1473 K for 0.6 ks, followed by quenching in water. The average prior austenite grain size, packet size, block thickness, sub-block thickness, and lath thickness were 350, 130, 13, 7, and 0.5 µm, respectively.

The microstructure was examined by optical microscope (OM) and SEM/EBSD. For the OM observations, the specimens were etched with 5% nital solution. The crystallography of the blocks and sub-blocks was evaluated by two EBSD systems, installed in a conventional SEM and a high resolution field emission SEM (FE-SEM).

In this study, the K–S variants in a packet were defined as shown in Table 1 and Fig. 2, which is the same definition as in the previous reports.[1,2)] The sub-blocks contain a single K–S variant, i.e. V1 to V6, whereas the blocks in a packet contain the V1-V4, V2-V5, and V3-V6 variant pairs.

In the present study, indexing of planes and directions was made with reference to the austenite. Since austenite does not remain after quenching, due to the fully martensitic transformation in the interstitial free steel, it is impossible to directly measure the orientation relationship between the martensite laths and austenite. The lath martensite is known to relate with austenite in the near K–S relationship, and the 24 variants of the lath martensite can form in an austenite grain.[1)] Taking the orientation relationship between the martensite laths and possible variants into consideration, the crystal orientation of the austenite can be estimated indirectly.[8)] According to the preliminary analysis, the estimated crystal orientation of the austenite was reliable with an error less than five degrees.

Table 1 Twenty four variants in K–S relationship with habit plane of each variant in a packet.[1)]

Variant #	Plate parallel	Direction parallel	Habit plane
1	$(111)\gamma$ // $(011)\alpha'$	$[\bar{1}01]\gamma$ // $[\bar{1}\bar{1}1]\alpha'$	$(575)\gamma$
2	$(111)\gamma$ // $(011)\alpha'$	$[\bar{1}01]\gamma$ // $[\bar{1}1\bar{1}]\alpha'$	$(575)\gamma$
3	$(111)\gamma$ // $(011)\alpha'$	$[01\bar{1}]\gamma$ // $[\bar{1}\bar{1}1]\alpha'$	$(755)\gamma$
4	$(111)\gamma$ // $(011)\alpha'$	$[01\bar{1}]\gamma$ // $[\bar{1}1\bar{1}]\alpha'$	$(755)\gamma$
5	$(111)\gamma$ // $(011)\alpha'$	$[1\bar{1}0]\gamma$ // $[\bar{1}\bar{1}1]\alpha'$	$(557)\gamma$
6	$(111)\gamma$ // $(011)\alpha'$	$[1\bar{1}0]\gamma$ // $[\bar{1}1\bar{1}]\alpha'$	$(557)\gamma$

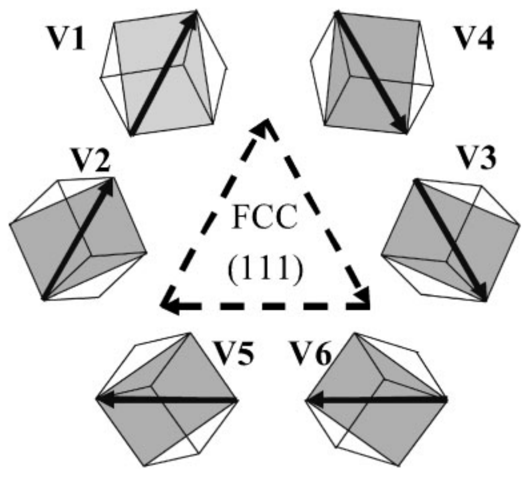

Fig. 2 Schematic illustration of K–S variant in a packet. One triangle and six cubes are close packed plane of austenite and unit cells of martensite. The broken arrows are closed packed direction in (111) of austenite. The solid arrows and gray planes are corresponding closed packed directions and planes of martensite. V1 to V6 are the number of the K–S variants determined in Ref. 1).

Serial sectioning images were obtained by combination of repeated sectioning and observation. The scanning pitch of electron beam for EBSD measurements was set at 500 nm. The specimens for the EBSD analyses were mechanochemically polished with colloidal silica (an abrasive) to obtain a smooth and damage-free specimen surface. The polishing depths during serial sectioning were determined by measuring the width of the Vickers indents. The microstructures were observed with 19 sections over an area of $250 \times 200\,\mu m^2$ and a total depth of 11 µm. Serial sectioning images were reconstructed using rendering software, IMOD.[9)]

3. Results and Discussion

3.1 Morphology of blocks and sub-blocks

Figure 3(a) shows a SEM image showing the typical low carbon lath martensite structure. The orientation image map (Fig. 3(b)) corresponding to the squared region in Fig. 3(a) suggests that the block boundaries that are marked with red lines are not flat, as reported previously.[2)] The orientation relationship between the blocks in a packet is $[011]\alpha'/49.5$–70.5 degrees, and that between the sub-blocks is $[011]\alpha'/10.5$ degrees. The block and sub-block boundaries are classified as high ($>15°$, shown by the red line) and low ($<15°$, shown by the black line) angle boundaries, respectively. The several blocks in the same region of Fig. 3(b) were colored based on the variants in the packet and shown in Fig. 3(c) as a variant map. V1-V4 pairs (shown in red and pink) and V2-V5 pairs (shown in sky blue and blue) were observed. However, no V3-V6 pairs, which are associated with the relaxation of the strain in the packet introduced by the martensitic transformation, were found. In the block, e.g., the V1-V4 block indicated with green broken lines, the sub-blocks with V1 exist dominantly, and the sub-blocks with V4 exist in V1 variant. Small amount of sub-blocks in a block such as V4 in Fig. 3(c), are defined as minor sub-blocks.

Figure 4(a) shows an orientation image map from a different area. The block boundaries are indicated by red lines, and each block was divided by sub-blocks, indicated by black lines; that is, orange (V1)-yellow (V4) sub-blocks, purple (V2)-violet (V5) sub-blocks, and blue (V3)-sky-blue (V6) sub-blocks are contained in the block. There are two types of minor sub-block morphologies as shown in Fig. 4(a)—elongated regions, which are parallel to block boundaries, indicated by "I" in 2D, and small equiaxed regions, indicated by "II" with an open circle. The elongated morphology is more than 20 µm in length and a few µm in width. The size of other elongated regions is a few tens of µm.

Figures 4(b) and (c) are orientation image maps at different depths, 3.6 and 5.4 µm, respectively, from that shown in Fig. 4(a). The small equiaxed sub-blocks indicated by red arrows in Fig. 4(a) become larger with change in the depth as shown in Fig. 4(b) and finally connect each other as shown in Fig. 4(c). The connected sub-block exhibited an elongated morphology nearly parallel to the block boundaries, such as region the "I". The yellow arrow in each map in Fig. 4 indicates the same position in the area. The yellow arrow in Fig. 4(a) indicated a point on the edge of blue elongated region. In Fig. 4(b), the blue elongated region was divided with increasing depth, and the elongated region pointed by the yellow arrow connected with the other elongated regions indicated by red arrows in Fig. 4(c). The change in the 2D morphology of the sub-blocks with depth suggests that 3D analysis is needed to reveal the shape of the sub-blocks.

In order to understand the sub-block morphology, 3D images were reconstructed. Figure 5(a) shows a top view of the block and sub-blocks from the normal direction of the specimen surface, which corresponds to the region marked by the broken green line in Fig. 3(c). A side view of the block and sub-blocks from the direction indicated by the arrow in Fig. 5(a) is shown in Fig. 5(b). Here, the block and sub-block boundaries are represented in black and colored, respectively. As mentioned above, the sub-block consists of V1 and V4 variants. The colored regions corresponding to the V4 (shown in pink in Fig. 3(c)) are shown in red, pink, blue, sky-blue, green, yellow and gray. The V4 variant regions are confined in the V1 variant and do not touch each other.

Using the 3D observations, the small equiaxed morphology from 2D observations looks like plate, which is indicated by circle in Fig. 5(c) and whose viewpoint is the same as that in Fig. 5(b). The plates, which are aligned parallel to the block boundaries, connect each other, and the section of connected plates in 2D observations becomes the elongated morphology, as shown in Fig. 5(c).

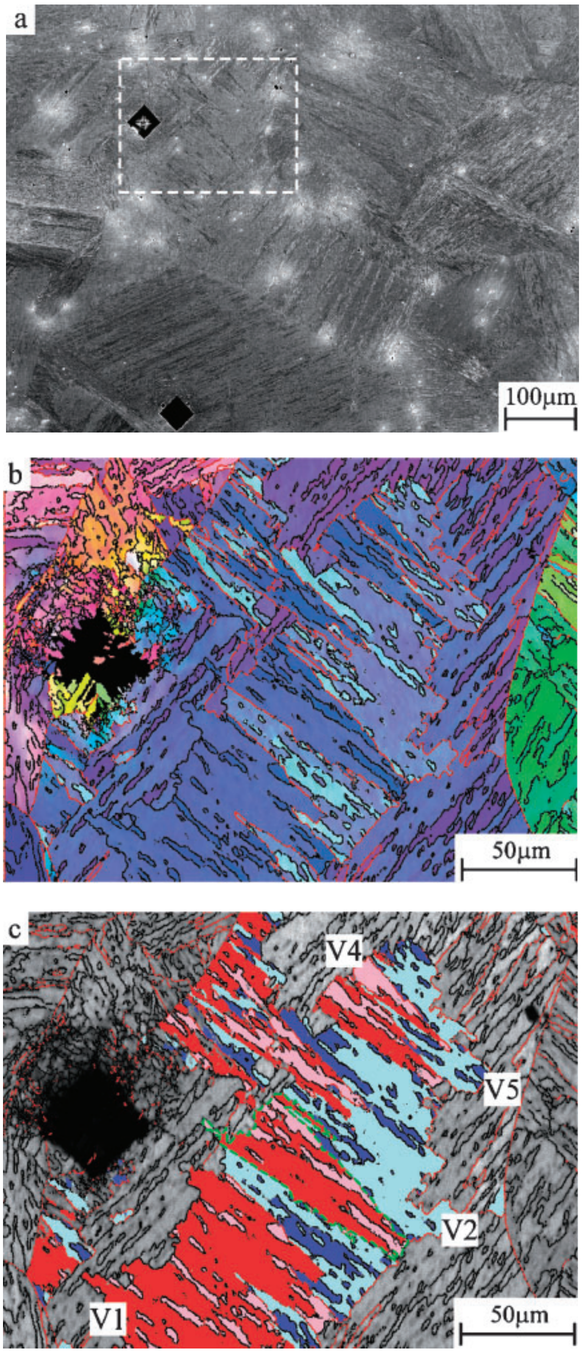

Fig. 3 SEM/EBSP measurement of the lath martensite; (a) SEM image, (b) orientation image map, and (c) K–S variant map. The black squares indicate Vickers hardness. In Fig. 3(b) and 3(c), the black and red lines show low angle (<15°) and high angle (>15°) boundaries, respectively. The colors in Fig. 3(c) show the K–S variants, red-V1, sky blue-V2, pink-V4, and blue-V5.

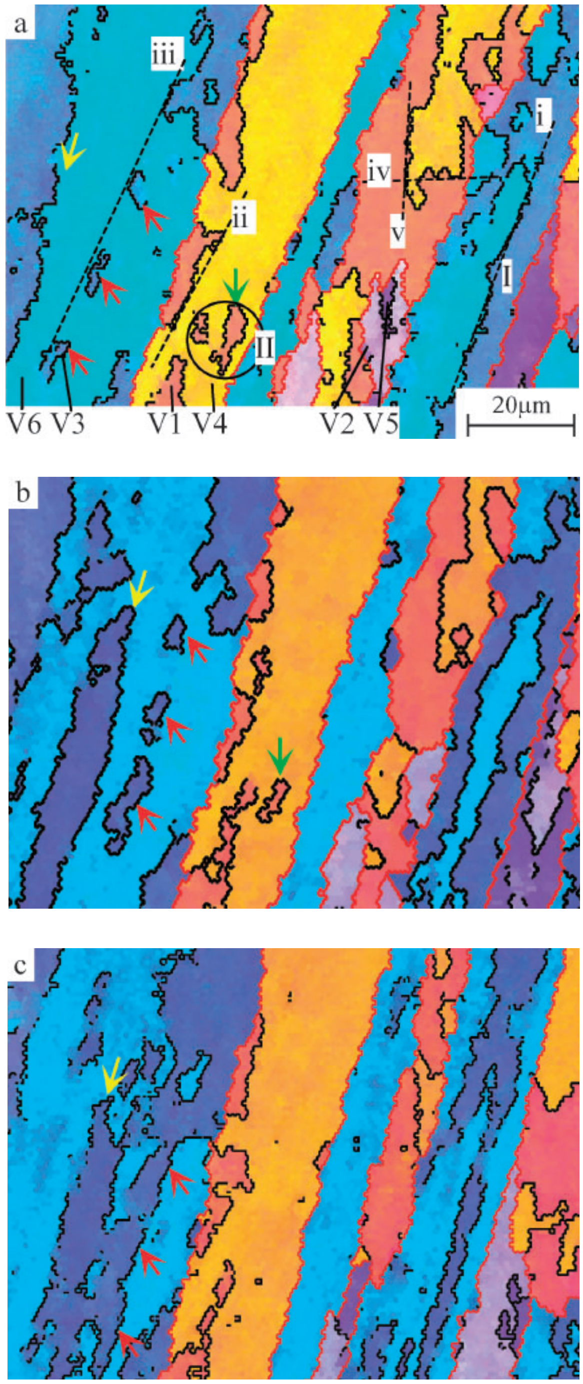

Fig. 4 Orientation image maps measured with SEM/EBSD of the lath martensite on the different depth: (a) 0 (original surface), (b) −3.6 and (c) −5.4 μm deep. The colors also indicate the K–S variants, orange-V1, purple-V2, blue-V3, yellow-V4, violet-V5, and sky blue-V6. The black and red lines show low angle (<15°) and high angle (>15°) boundaries, respectively. Broken lines from i to v are traces of sub-block boundaries. The red, green, and yellow arrows indicate the same sub-blocks.

3.2 The habit plane and orientation relationship of sub-blocks

2D observations show that the sub-block boundaries are parallel to block boundaries. It suggests that minor sub-block surfaces are near the habit planes of the blocks. To determine the sub-block boundaries, the misorientation angles between the normal of the habit planes and the trace of the sub-block boundaries were calculated. This is because the trace must be perpendicular to the normal of the habit planes. The sub-block boundaries contain specific planes, such as i, ii, iii, iv, and v, as shown in Fig. 4(a). Table 2 is the result of the trace analysis for the sub-block boundaries, i, ii, iii, iv and v. The planes, traced by i, ii, iii, and v, are $(111)\gamma$, $(557)\gamma$, $(575)\gamma$, and $(755)\gamma$, which are the habit plane of lath martensite with V1 to V6, as shown in Table 1.[1)] The sub-block boundary, iv, could not be indexed because it is difficult to measure the elongated direction and index of surfaces of the minor sub-blocks by 2D observations.

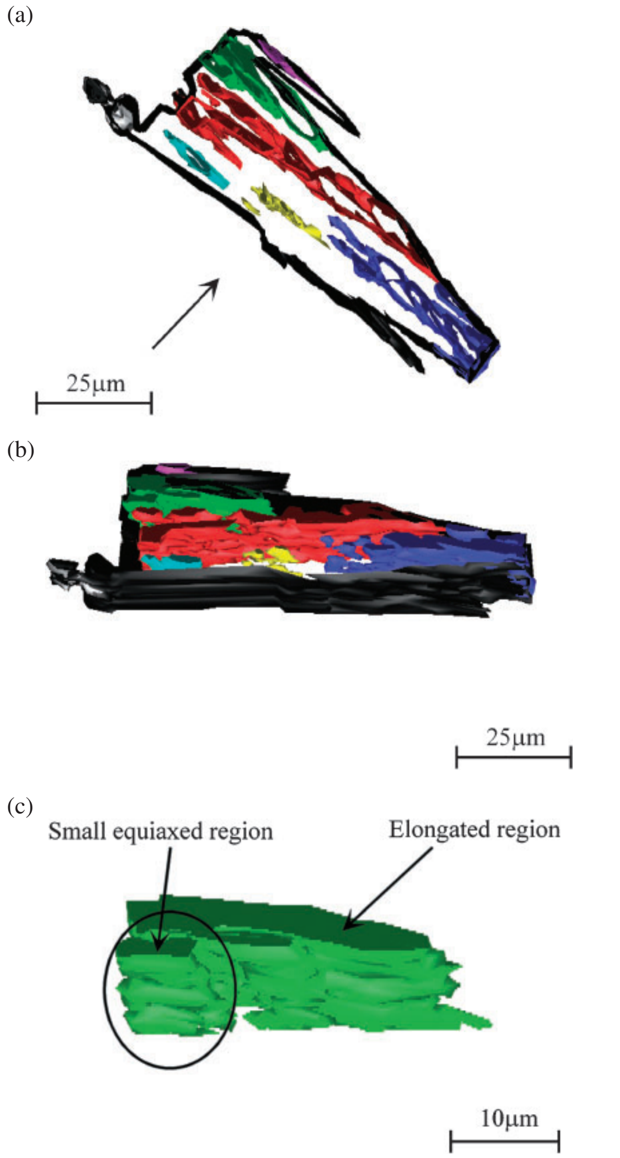

Fig. 5 The 3D image of a block surrounded with green broken lines in Fig. 3(c) on (a) top view from normal direction of specimen surface, (b) side view from arrow direction in Fig. 5(a), and (c) green colored sub-block in Fig. 5(b). The black ribbon corresponds to block boundary and other colored ribbons correspond to sub-block boundaries. The sub-blocks encircled with colored ribbons and the white regions of the sub-blocks contain the laths with V4 and V1 variants, respectively.

Table 2 Misorientation angles between traces and habit planes of lath martensite.

Trace #	Angle from trace to normal direction of habit plane [degree]			
	$(111)\gamma$	$(575)\gamma$	$(755)\gamma$	$(557)\gamma$
i	89	81	83	90
ii	88	89	75	86
iii	82	85	68	79
iv	70	39	46	55
v	90	78	86	88

The surface and elongated direction were analyzed by two-face analysis using 3D measurements. Figure 6(a) shows one of the sub-blocks, which is shown in red in Fig. 5(a). The minor sub-blocks have two types of flat sub-block boundaries, $(0.4110\ 0.5364\ 0.7371)\gamma$ and $(0.460\ 0.718\ 0.522)\gamma$, indicated by blue arrows. Another result of the sub-block boundary is $(0.563\ 0.622\ 0.544)\gamma$ as indicated by a blue arrow (as shown in Fig. 6(b)). The surfaces are near $(111)\gamma$ because the misorientation angles between $(111)\gamma$ and $(0.4110\ 0.5364\ 0.7371)\gamma$, $(0.460\ 0.718\ 0.522)\gamma$, and $(0.563\ 0.622\ 0.544)\gamma$ are 13, 11, and 3 degrees, respectively. The boundaries of the sub-block plate are almost parallel to $(111)\gamma$, which are the same results as from 2D analysis. In Fig. 6(b), the sky blue colored sub-block has two elongated horn like parts, which are indicated by green and red arrows. The elongated directions in green and red were close to $[10\bar{1}]\gamma$ and $[01\bar{1}]\gamma$, which correspond to the close packed directions of V1 and V4, respectively. Note that the boundary and growth direction of the sub-block plate are close to those of martensite laths in a block.

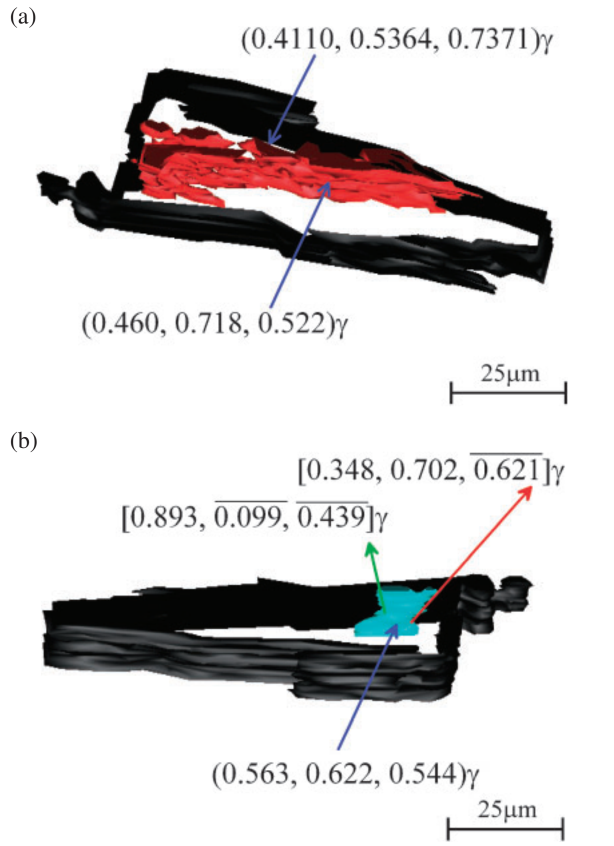

Fig. 6 Crystallographic analysis of the sub-block colored with (a) red and (b) sky blue as shown in Fig. 5(a) and (b). The blue arrows indicate the habit plane, whereas the green and red lines indicate elongated direction of the sub-block branches.

4. Conclusions

Martensite sub-blocks were analyzed with 2D and 3D observations using the serial sectioning-EBSP technique. The following conclusions are derived from the results.

(1) The blocks consist of one dominant sub-block and many minor sub-blocks, of which the dominant and other sub-blocks have different K–S variants. The orientation

relationship between the dominant and minor sub-blocks is $[011]\alpha'/10.5$ degrees.
(2) The minor sub-blocks exhibit a plate morphology, with 10 µm wide, and they connect with the other within a block.
(3) The habit plane and elongated direction of the sub-block plate are close to $\{111\}\gamma$ and $\langle 101\rangle\gamma$, respectively, which are commonly observed for martensite laths.

Acknowledgments

The financial support of the Ministry of Education, Culture, Sports, Science and Technology of Japan through a Grant-in-Aid for Scientific Research (C) No. 20560696 (2008–2010) and the ISIJ Innovative Program for Advanced Technology are gratefully acknowledged. Special thanks are given to Prof. X. Huang (RISØ national laboratory, the Technical University of Denmark, Denmark) for useful discussions.

REFERENCES

1) S. Morito, H. Tanaka, R. Konishi, T. Furuhara and T. Maki: Acta Mater. **51** (2003) 1789–1799.
2) S. Morito, X. Huang, T. Furuhara, T. Maki and N. Hansen: Acta Mater. **54** (2006) 5323–5331.
3) F. B. Pickering: *Hardenability Concepts with Applications to Steel*, (American Institute of Min. Metall. and Petroleum Eng., Warrendale (PA), 1978) pp. 179–228.
4) S. Matsuda, T. Inoue, H. Mimura and Y. Okamura: Proc. Int. Sympo. on Toward Improved Ductility and Toughness, Kyoto, Japan, (The Iron and Steel Inst. of Japan, 1971) pp. 45–66.
5) S. Morooka, Y. Tomota, Y. Adachi, S. Morito and T. Kamiyama: Tetsu-to-Hagane **94** (2008) 313–320.
6) A. C. Lewis, J. F. Bingert, D. J. Rowenhorst, A. Gupta, A. B. Geltmacher and G. Spanos: Mater. Sci. Eng. A **418** (2006) 11–18.
7) D. J. Rowenhorst, A. Gupta, C. R. Feng and G. Spanos: Scr. Mater. **55** (2006) 11–16.
8) T. Furuhara, H. Kawata, S. Morito, G. Miyamoto and T. Maki: Metall. Mater. Trans. A **39A** (2008) 1003–1013.
9) J. R. Kremer, D. N. Mastronarde and J. R. McIntosh: J. Struct. Biol. **116** (1996) 71–76.